Potential Energy Surface for the Acid- and BF_3-Catalyzed Rearrangement of Methylpropene Oxide

James M. Coxon,* Aaron J. Thorpe, and William B. Smith†

Department of Chemistry, University of Canterbury, Christchurch, New Zealand

Received July 26, 1999

The acid- and BF_3-catalyzed rearrangement of methylpropene oxide to methylpropanal has been investigated by density functional methods. Isotope effects are calculated and are consistent with the reaction occurring via a carbocation intermediate followed by a 1,2-hydride shift. Inverse secondary isotope effects for hydride migration reflect a combination of changes in C1−H(D) stretching and out-of-plane bending frequencies with a stronger force constant of the nonmigrating C1−H bond at the transition structure than in the carbocation. Gas-phase DFT(B3LYP)/6-31G* level calculations favor a geometry of the carbocation with the boron of BF_3 below the plane of the carbon framework while B3LYP/6-31G*(SCI−PCM) single point solvation calculations favor a geometry with the boron in the plane. From this latter conformation hydride migration to either face of the carbocation is equally favored. The transition structure for hydride (deuteride) migration is early. A calculated correction applied to the experimentally observed result ($M_H/M_D = 1.92$) gives a primary isotope effect for the reaction ($k_H/k_D = 1.56$) close to the theoretically calculated value ($k_H/k_D = 1.68$).

Introduction

Epoxide ring opening has been implicated in the carcinogenic properties associated with activated epoxides. Epoxides are also important synthetic intermediates, and therefore, understanding their reaction chemistry and mechanism of reaction is of some importance. The rearrangement of methylpropene oxide with BF_3 gives methylpropanal, which is trapped by further reaction with epoxide as dioxolanes.[1] Previous work[2,3] in our laboratory on the BF_3-catalyzed rearrangement of 1-deutero-2-methyl-1,2-epoxypropane **1** in carbon tetrachloride showed the formation of the deuterated methylpropanals (17%) **3** and **4**, along with a mixture of dioxolones (79%) **5** and **6** and 1,4-dioxane (4%) **7** (Figure 1).

The mechanism for formation of **3** and **4** from **1** was considered to occur by ring opening of epoxide coordinated to Lewis acid to give carbocation **2**, followed by a 1,2-hydride shift. No deuterium was lost in the rearrangement, thereby excluding an enol intermediate in the reaction and also showing that the aldehyde was not enolized under the reaction conditions. The results are therefore consistent with the rearrangement involving a 1,2-hydride migration. A primary deuterium isotope effect[4] is observed[3] with preferential migration of hydride vs deuteride to the carbocation center of **2** (i.e. **4** > **3**). Since the aldehydes are unstable on exposure to air and readily undergo oxidation, the ratio of hydride (from a carbon containing a deuterium) to deuteride migration (from a carbon containing a hydrogen) was established from integration of the NMR spectrum of the dioxolans **5** and **6**. This ratio, M_H/M_D, was established as 1.92 (standard deviation 0.04). The primary isotope effect, k_H/k_D, for the hydride (from a carbon containing hydrogen)/deuteride (from a carbon containing hydrogen) shift could be derived[5] from M_H/M_D if the isotope effect implicit in all the internal H/D-competitive reactions were allowed for. These corrections are calculated in the present study.

* Corresponding author. E-mail: J.Coxon@chem.canterbury.ac.nz.
† Usual address: Chemistry Department, Texas Christian University, Fort Worth, TX 76129.

(1) Yandovskii, Y. N.; Temnikova, T. *L J. Org. Chem. USSR* **1968**, *33*, 1695. Blackett, B. N.; Coxon, J. M.; Hartshorn.; Lewis, A. J.; Little, G. R.; Wright, G. J. *Tetrahedron* **1970**, *26*, 1311. O^{18} studies show that the mechanism of dioxolane formation involves attack of a carbonyl (the aldehyde) on the epoxide, not the reverse (Coxon, J. M.; Hartshorn, M. P.; Sutherland, B. L. S. *Aust J. Chem.* **1974**, *27*, 679). The epimeric 6-*tert*-butyl-1-oxaspiro[2,5]octanes react with O^{18}-labeled acetone to give epimeric mixtures of dioxolanes with the O^{18} attached to the cyclohexyl ring, consistent with a preference for axial attack, an intermediate tertiary cation coupled with a preference of acetone attack with inversion.

(2) Coxon, J. M.; Hartshorn, M. P.; Swallow, W. H. *Aust. J. Chem.* **1973**, *26*, 2521.

(3) Blackett, B. N.; Coxon, J. M.; Hartshorn, M. P.; Richards, K. E. *Aust J. Chem.* **1970**, *23*, 839.

(4) Isotope effects reflect changes in reaction rate as a result of isotopic substitution that are related to structural changes in reactant and transition structure and thereby provide mechanistic information. They depend largely on the nature of the bonds being formed or broken, reflecting changes in the vibrational frequencies between the reactant and transition structure which are in turn related to the force constants and atomic masses of the isotopes. The vibrational modes which exhibit the greatest change between the reactant and transition structure contribute most to a KIE. Kinetic isotope effects are termed "normal" if $k_H/k_D > 1$ and inverse when $k_H/k_D < 1$. When the bond to an isotope is broken during the course of a reaction, a primary isotope effect (PKIE or PIE) is observed for that step of the reaction process and its magnitude is determined largely from changes in stretching vibrations. Secondary kinetic isotope effects (SKIEs or SIEs) arise when the bond to the isotope is at the reaction center but is not broken during the course of a reaction but influences nearby vibrations. The connection between secondary isotope effects and hybridization changes at an isotopically substituted reaction center was first investigated by Streitweiser (Streitweiser. A., Jr.; Jagow, R. H.; Fahey, R. C.; Suzuki, S. *J. Am. Chem. Soc.* **1958**, *80*, 2326) who established that changes in the Cα−H(D) out-of-plane bending frequencies are the most important. For example for an S_N2 reaction, where hybridization changes from sp^3 to sp^2 at the center undergoing reaction, a normal SKIE > 1 is observed when deuterium is substituted at the reaction centre. An inverse SKIE < 1 occurs when hybridization changes from sp^2 to sp^3 (e.g. Diels−Alder reaction). Recent work has demonstrated that changes in stretching as well as bending vibrations can be important in SKIEs (Zhao, X. G.: Tucker S. C.; Truhlar, D. G. *J. Am. Chem. Soc.* **1991**, *113*, 826. Zhao, X. G.; Lu, D.-H.; Liu, Y.-P.; Lynch, D. G.; Truhlar, D. G. *J. Chem. Phys.* **1992**, *97*, 6369).

(5) The aldehyde is not completely converted into dioxolane. The isotope effect for reaction of aldehyde with epoxide will be small.

10.1021/jo9911802 CCC: $18.00
Published on Web 12/02/1999

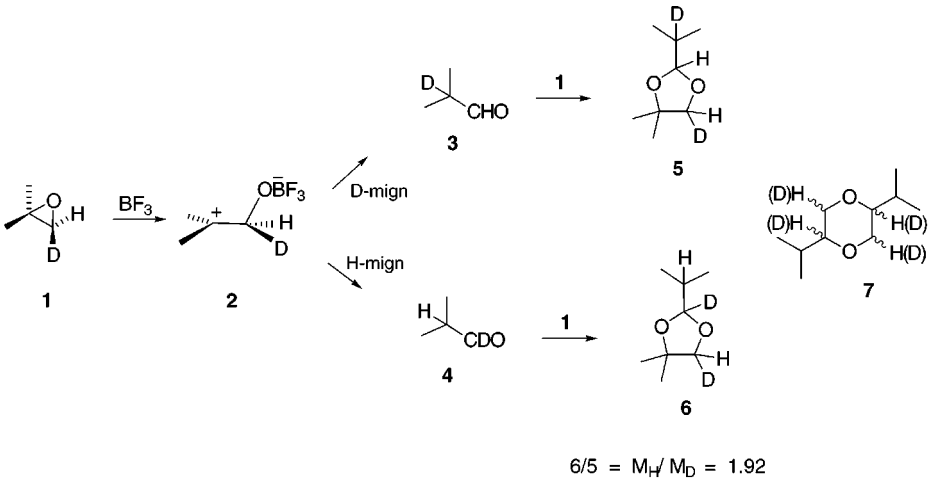

Figure 1. The rearrangement of **1** with BF_3, via intermediate **2** to aldehydes **3** and **4**, dioxolones **5** and **6** and 1,4-dioxane **7**.

We now report a study of acid- and BF_3-catalyzed rearrangement of methylpropene oxide to methylpropanal by density functional methods. Isotope effects are calculated,[4] compared to experimental values, and used to elaborate the mechanism of rearrangement. The vibrational frequencies which provide the greatest contribution to the magnitude of selected isotope effects are analyzed in detail.

Computational Methods

Exploratory calculations of the potential energy surface were carried out at the semiempirical level,[6] followed by ab initio calculations with the 6-31G* basis set. Electron correlation was accounted for through the use of gradient-corrected hybrid density functional DFT(B3LYP)/6-31G*[7] theory. Intrinsic reaction coordinate (IRC) calculations at the B3LYP/6-31G* level were employed to determine the relevance of the stationary points on the potential energy surface. Theoretical primary and secondary isotope effects can be calculated by either eqs 4 and 5, described in detail below, using vibrational frequencies and the Gibbs free energy data from frequency calculations using the Gaussian94[8] program. Vibrational frequencies were computed at 298.15 K and scaled by 0.961 and 0.893 for the B3LYP/6-31G* and HF/6-31G* levels accordingly.[9] Single point solvation calculations were performed at the B3LYP/6-31G* level in conjunction with the self-consistent isodensity polarized continuum model[10] (SCI−PCM) within Gaussian94 and with a dielectric constant of 2.23.[11]

Transition state theory in conjunction with statistical mechanics is the method of choice for the interpretation of kinetic isotopes effects.[12] Bigeleisen and Mayer derived eq 4,[13,14] which, in the absence of symmetry number effects, contains terms for all vibrations of the reactant and transition structure.

$$\left(\frac{S_2}{S_1}\right)f_{\text{react}} = \prod_i^{3N-6}\frac{u_{2i}}{u_{1i}}\frac{[1-\mathrm{e}^{-u_{1i}}]}{[1-\mathrm{e}^{-u_{2i}}]}\exp\left[\sum_i^{3N-6}\frac{(u_{1i}-u_{2i})}{2}\right]$$

$$\left(\frac{S_2}{S_1}\right)f_{\text{TS}} = \frac{V_{1\text{L}^\dagger}}{V_{2\text{L}^\dagger}}\prod_i^{3N-7}\frac{u_{2i}}{u_{1i}}\frac{[1-\mathrm{e}^{-u_{1i}}]}{[1-\mathrm{e}^{-u_{2i}}]}\exp\left[\sum_i^{3N-7}\frac{(u_{1i}-u_{2i})}{2}\right]$$

$$\frac{k_{\text{H}}}{k_{\text{D}}} = \frac{(s_2/s_1)f_{\text{react}}}{(s_2/s_1)f_{\text{TS}}}$$

$$u_i = h\nu_i/k\text{T} = 1.4387\ \nu_i/\text{T} \qquad (4)$$

The kinetic isotope effect is expressed as the ratio of the reduced isotopic partition function of the reactant $(S_2/S_1)f_{\text{react}}$ divided by the reduced isotopic partition

(6) Dewar, M. J. S.; Zoebisch, E. G.; Healy, E. F.; Stewart, J. J. P. *J. Am. Chem. Soc.* **1985**, *107*, 3902.

(7) Becke, A. D. *Phys. Rev.* A **1988**, *38*, 3098. Becke, A. D. *J. Chem. Phys.* **1993**, *98*, 1372. Lee, C.; Yang, W.; Parr, R. G. *Phys. Rev.* B **1988**, *37*, 785.

(8) Frisch, M. J.; Trucks, G. W.; Schlegel, H. B.; Gill, P. M. W.; Johnson, B. G.; Robb, M. A.; Cheeseman, J. R.; Keith, T.; Petersson, G. A.; Montgomery, J. A.; Raghavachari, K.; Al-Laham, M. A.; Zakrzewski, V. G.; Ortiz, J. V.; Foresman, J. B.; Cioslowski, J.; Stefanov, B. B.; Nanayakkara, A.; Challacombe, M.; Peng, C. Y.; Ayala, P. Y.; Chen, W.; Wong, M. W.; Andres, J. L.; Replogle, E. S.; Gomperts, R.; Martin, R. L.; Fox, D. J.; Binkley, J. S.; Defrees, D. J.; Baker, J.; Stewart, J. P.; Head-Gordon, M.; Gonzalez, C.; Pople, J. A. Gaussian94, Revision D.2; Gaussian, Inc., Pittsburgh, PA, 1995.

(9) Foresman, J. B.; Frisch, A. *Exploring Chemistry with Electronic Structure Methods*, 2nd ed.; 1996; Chapter 4, p 62.

(10) Foresman, J. B.; Keith, T. A.; Wiberg, K. B.; Snoonian, J.; Frisch, M. J. *J. Phys. Chem.* **1996**, *100*, 16098.

(11) *Handbook of Chemistry and Physics*, 60th ed.; Weast, R. C., Ed.; CRC Press: Boca Raton, FL, 1980; p E55.

(12) From absolute rate theory and statistical mechanics, the total energy of a molecule can be expressed as the sum of individual partition functions, Q, representing translational, rotational, vibrational and electronic energy levels: $Q = Q_{\text{trans}}Q_{\text{rot}}Q_{\text{vib}}Q_{\text{elec}}$ (eq 1), where Q is expressed as $Q = \sum p_{ie_i}{}^{-e_i/KT}$ and is the summation over all energy states. Isotopic substitution has little influence on the reduced mass of a molecule and so Q_{elec} can be ignored since the potential energy surface and electronic levels remain essentially unchanged. The translational and rotational partition functions can also be ignored since in most cases the molecular masses and moments of inertia give no appreciable contribution to the isotope effect. An expression for the equilibrium constant involving the partition functions Q for the reactant and $Q^\dagger$ representing the activated complex (transition structure) is defined as $K^\dagger = [Q^\dagger/Q(\text{reactant})]\mathrm{e}^{-E_a/kT}$ (eq 2) and a kinetic isotope effect is expressed as $k_{\text{H}}/k_{\text{D}} = K_{\text{H}}{}^\dagger/K_{\text{D}}{}^\dagger = (Q_{\text{H}}{}^\dagger/Q_{\text{D}}{}^\dagger)(Q_{\text{D}}(\text{reactants})/Q_{\text{H}}(\text{reactants}))$ (eq 3).

(13) Bigeleisen, J.; Mayer, M. G. *J. Chem. Phys.* **1947**, *15*, 261−267. Bigeleisen, J. *J. Chem. Phys.* **1949**, *17*, 675. Bigeleisen, J.; Wolfsberg, M. *Adv. Chem. Phys.* **1958**, *1*, 15.

(14) The subscripts 1 and 2 refer to the atomic masses of hydrogen and deuterium, respectively, and u_i is defined by the parameters ν_i, a normal−mode harmonic frequency, Boltzmann's constant, k, and the absolute temperature, T. The reactant molecule is represented by $3N - 6$ normal vibrational modes where N is the number of atoms in the molecule. For transition structures there are $3N - 7$ normal vibrational modes since the imaginary frequency is not treated as a proper vibrational mode and any movement away from the saddle point results in decomposition along the reaction coordinate.

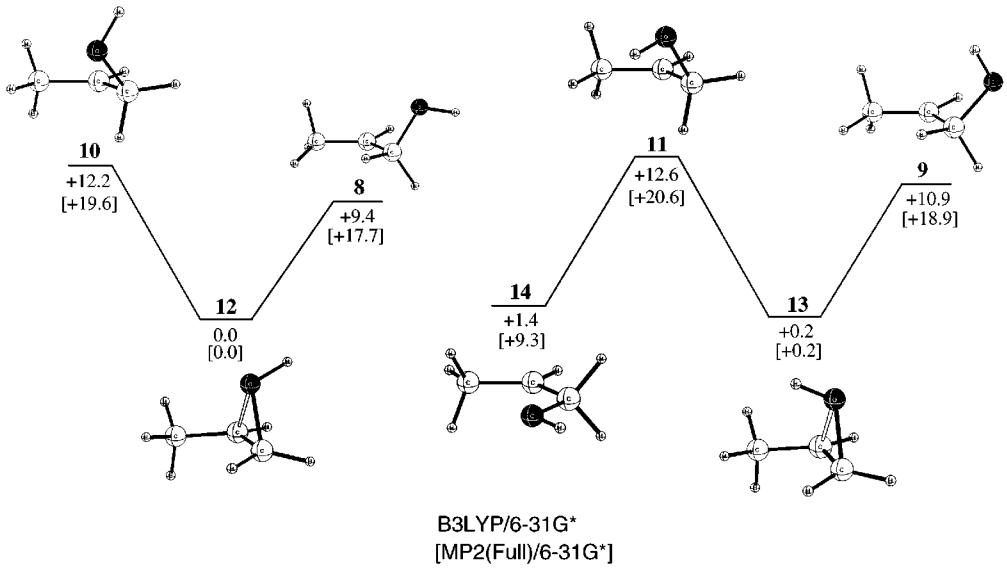

Figure 2. Optimized transition structures (MP2(Full)/6-31G*) for the rearrangement of protonated propene oxide. Energies (kcal/mol) at the B3LYP/6-31G* and MP2(Full)/6-31G* levels of theory. Solid connecting lines show the result of IRC calculations. **8**−**10** connect by IRC calculations to protonated aldehyde.

function of the transition structure (S_2/S_1)f_{TS}, and includes a term ($V_{1L}{}^{\dagger}$ /$V_{2L}{}^{\dagger}$) representing the ratio of imaginary frequencies of the nondeuterated and deuterated transition structures. Standard ab initio molecular orbital programs are used to calculate reactant and transition structure geometries and their associated normal-mode vibrational frequencies.

An alternative and simpler procedure for calculating kinetic isotope effects, utilizing the difference in Gibbs free energy between the nondeuterated and deuterated reactant and transition structure and summary data from the Gaussian94 output substituted directly into eq 5, necessarily gives the same results.[15,16]

$$k_H/k_D = \exp[-(\Delta G_H - \Delta G_D)/RT] \qquad (5)$$

where $\Delta G = G^{\dagger} - G^{r}$ and † = transition structure and r = reactant.

While the use of eq 4 requires more specific input data than eq 5, it is useful as it allows the frequencies which contribute most to the isotope effect to be determined. Both methods, which are in fact equivalent,[16] are used in the present study of the stationary points on the potential energy surface for the rearrangement of **1** to **3** and from **1** to **4** with acid and BF_3. The appropriate primary and secondary isotope effects for the stationary points directly involved with the hydride shift to aldehyde are calculated and compared with experiment.

Results and Discussion

Rearrangement of Protonated Propene Oxide and Methylpropene Oxide with Acid. We have previously reported the potential energy surface for the rearrangement of protonated propene oxide to propanal at the MP2(full)/6-31G* level.[17] Since we reported this study, density functional methods have been shown to be cost-effective. We have therefore computed the B3LYP/6-31G* geometries and energies of the stationary points on the surface to make comparison with the present study.

A total of four transition structures **8**−**11** were established (MP2/6-31G*) from the rearrangement of the two protonated epoxide invertomers[18] **12** and **13** (Figure 2). Intrinsic reaction coordinate calculations (MP2/6-31G*) for each of the transition structures **8**−**11** led to the appropriate protonated epoxides **12** and **13**. In the other direction the three lowest energy transition structures **8**−**10** gave protonated aldehyde with each IRC showing a rearrangement by 1,2-hydride shift in a concerted asynchronous reaction pathway.[19] The highest energy transition structure **11** led to a symmetrical carbocation intermediate **14**, where both C1 protons are equally positioned to migrate via a 1,2-hydride shift. The optimized stationary point geometries at the B3LYP/6-31G* level remain essentially the same as at the MP2(Full)/6-31G* level. However, electronic energy barriers calculated by the former are substantially smaller (Figure 2).

The stationary points for the rearrangement of protonated methylpropene oxide to protonated methylpropanal are shown in Figure 3. Addition of a proton to methylpropene oxide produces an oxonium cation **15**. The C2−O bond is lengthened (1.691 Å) relative to the C1−O bond (1.495 Å), reflecting the preference for opening at the tertiary center which occurs with rotation about the C1−C2 bond in either direction to give transition structures **16** and **17**. The former is the lower in energy (0.3 kcal/mol) with a barrier of 2.7 kcal/mol (B3LYP/6-31G*) and is substantially lower than the analogous barriers for the

(15) The values required in the equations are contained in the output of ab initio frequency calculations.

(16) *Cautionary comment:* If the frequency data for the starting structure and transition structure (from which the checkpoint files are used for an isotope calculation) are not specifically scaled (i.e. scale factor 1.0) and used in conjunction with the isotope calculation frequency data where a scale factor of 1.0 is not specified, this leads to erroneous isotope effect calculations. If a scale factor of 1.0 is not specified in the Gaussian94 program input file for the isotope calculation, the program automatically assigns a scale factor of 0.8929. This results in the isotope effects calculated by the alternative procedure to be in apparent conflict.

(17) Coxon, J. M.; Maclagan, R. G. A. R.; Rauk, A.; Thorpe, A. J.; Whalen, D. *J. Am. Chem. Soc.* **1997**, *119*, 4712.

(18) The term "invertomer" has been coined to describe the diastereomers resulting from positioning of a proton on either face of an epoxide. George, P.; Bock, C. W.; Glusker, J. P. *J. Phys. Chem.* **1990**, *94*, 8161.

(19) See Supporting Information of ref 17.

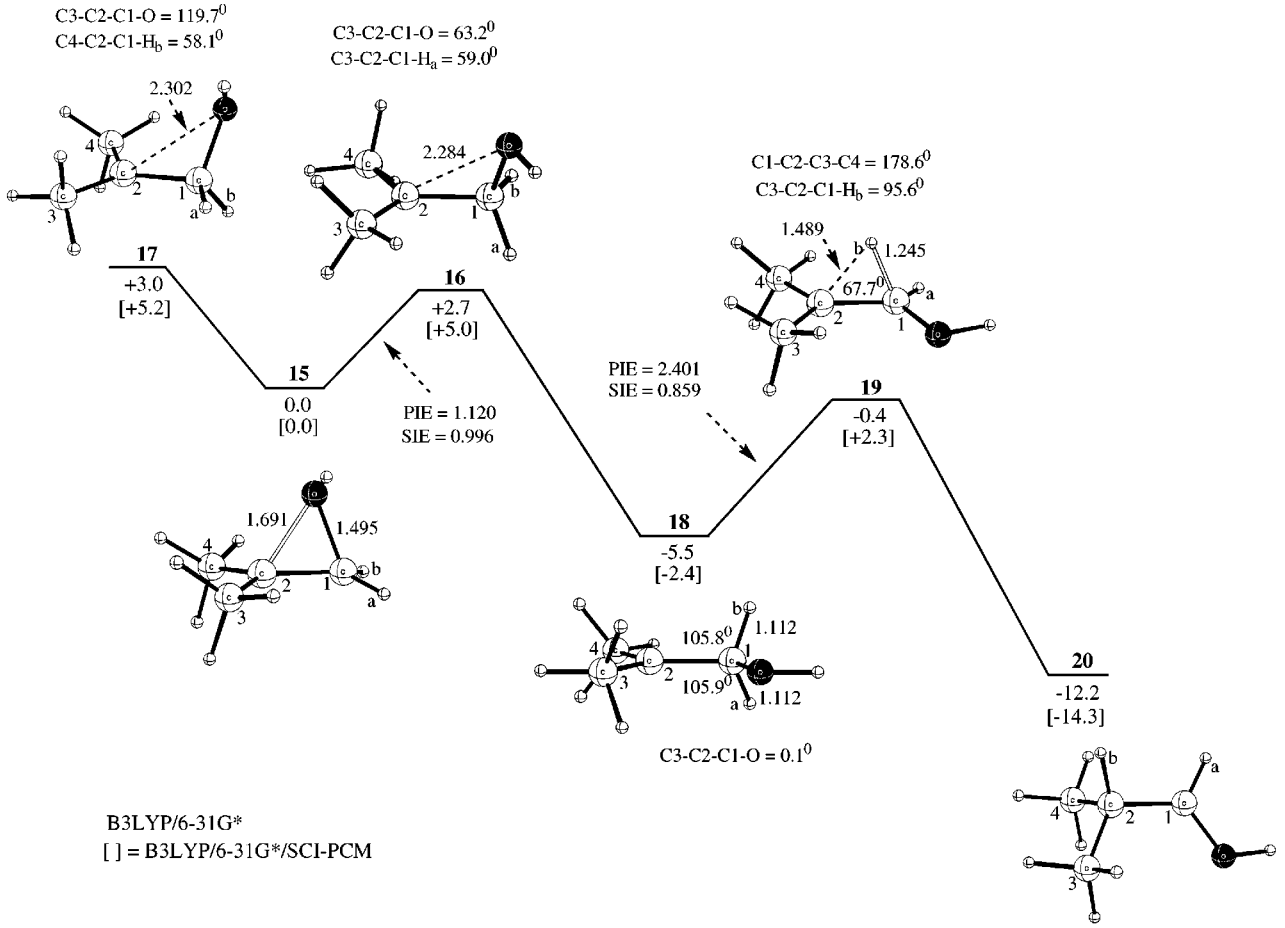

Figure 3. The rearrangement of **15** to **20**. Energies in kcal/mol relative to **15** include a ZPVE correction. Bond lengths in Å. Solid connecting lines show the result of IRC calculations.

ring opening of protonated propene oxide [the change in electronic energy for the lowest energy pathway is 9.4 kcal/mol (B3LYP/6-31G*) or 17.7 kcal/mol (MP2(Full)/6-31G*)].

A C1−H has proceeded to overlap with the p-orbital of the carbocation in **16**, and **17**, but the bonds are not lengthened and the H−C1−C2 bond angles remain tetrahedral (**16**, H_a−C1 = 1.100 Å and H_a−C1−C2 = 109.6°, **17**, H_b−C1 = 1.099 Å and H_b−C1−C2 = 109.6°). For transition structure **16**, hyperconjugative stabilization of the carbocation occurs with a hydrogen on both methyls (H−C4−C2 = 105.1°, C4−H = 1.111 Å and H−C3−C2 = 106.3°, C3−H = 1.107 Å) with the orientation of the hydrogens antiperiplanar. Hyperconjugation also occurs in transition structure **17** (H−C4−C2 = 103.8°, C4−H = 1.112 Å and H−C3−C2 = 111.6°, C3−H = 1.100 Å).

An IRC calculation from transition structure **16** gave protonated epoxide **15** in one direction along the reaction coordinate and in the other direction, a planar carbocation intermediate **18**. The cation is stabilized relative to an analogous species from propene oxide by the addition of the methyl group at C2. Both C1 protons exhibit hyperconjugation with the C2 carbocation and are equally disposed to migrate. A transition structure **19** for 1,2-hydride migration from **18** to aldehyde **20** was identified and the connection between the three structures was confirmed by an IRC calculation. The 1,2-hydride shift is well-advanced in transition structure **19** with a C1−C2−H_b angle of 67.7° showing H_b to be nearly equally positioned between C1 and C2 and almost aligned with the p-orbital of the near-planar C2 cation. The C1−H_b bond is substantially lengthened in comparison with the analogous bond length in **18**.

The calculated primary and secondary isotope effects (PIE and SIE) are given in Table 3 along with geometrical parameters representative of the transition structures. The isotope effects calculated by using eqs 4 and 5 are necessarily identical in value.[16,20]

The position of the transition structure along the reaction coordinate reflects the force constants for the forming/breaking bonds. A 1,2-hydride shift requires bending of C2−C1−H from near tetrahedral in intermediate **18** to 67.7° in transition structure **19** and as a consequence the differences in bending modes make an important contribution in the magnitude of the isotope effect.[21]

Quantum mechanical tunneling has a more pronounced effect on primary than on secondary isotope effects and a number of proceedures have been devel-

(20) The magnitude of a primary kinetic isotope effect is determined by two aspects of the transition structure geometry. For a three-center transition structure model, a maximum isotope effect is observed when the C−H−X is linear and the hydrogen positioned "*midway*" between the C and X atoms. An asymmetric transition structure can be ascribed as "early" or "late."

C···H·····X C·····H···X C·····H···X

'*early*' TS '*symmetrical*' TS '*late*' TS

Table 1. Energies of Stationary Points [ZPC scaled by 0.961 (B3LYP) and 0.893 (HF)]

		energy (au)	ZPC (au)	energy + scaled ZPC (au)	imaginary frequencies. (i cm^{-1})	energy relative to minima **15**
			Transition Structure			
H^+						
16	optimized					
	B3LYP/6-31G*	−232.74694	0.12246	−232.62926	158.8	2.7
		−232.79896[a]				5.0
17	optimized					
	B3LYP/6-31G*	−232.74642	0.12234	−232.62886	142.3	3.0
		−232.79860[a]				5.2
19	optimized					
	HF/6-31G*	−231.27333	0.13039	−231.15680	760.8	0.3
	B3LYP/6-31G*	−232.75119	0.12168	−232.63426	637.9	−0.4
		−232.80322[a]				2.3
			Minima			
H^+						
15	optimized					
	HF/6-31G*	−231.27756	0.13468	−231.15730		0.0
	B3LYP/6-31G*	−232.75432	0.12559	−232.63363		0.0
		−232.80693[a]				0.0
18	optimized					
	HF/6-31G*	−231.28822	0.13079	−231.17143		−8.9
	B3LYP/6-31G*	−232.75956	0.12192	−232.64240		−5.5
		−232.81078[a]				−2.4
20	optimized					
	HF/6-31G*	−231.30390	0.14147	−231.17757		−12.7
	B3LYP/6-31G*	−232.77439	0.12631	−232.65301		−12.2
		−232.82970[a]				−14.3

[a] B3LYP/6-31G* (SCI-PCM) single point calculations. A dielectric constant of 2.23 (CCl_4) was used at 298.15 K.

oped[22] to calculate tunneling, which is more important the higher the activation barrier. The formula proposed by Bell[23] has been used in the present study to establish the importance or otherwise of tunneling:

$$\left(\frac{k_H}{k_D}\right)_{corr} = \frac{Q_t(H)}{Q_t(D)}\frac{k_H}{k_D} \quad \text{with} \quad Q_t = \frac{0.5u_i^{\dagger}}{\sin 0.5u_i^{\dagger}} \qquad (6)$$

The tunneling effects calculated using eq 6 are minute and result in no change to the isotope effects presented in Table 3, consistent with the low activation barriers for the 1,2-hydride shift. Although the transformation from **15** to **18** via transition structure **16** is the rate-determining step on the potential energy surface (Figure 3), at the transition structure, the hydride has not started to migrate though, there is some C1−H hyperconjugation with the C2 carbocation. Early experimental work on the acid-catalyzed rearrangement of exocyclic epoxides requires that the reaction partitions predominantly to a pathway involving a carbocation intermediate.[24]

Primary and secondary isotope effects were determined by replacing H_a and H_b respectively with deuterium. The calculated primary isotope effect for H_a, the proton most aligned with the developing cation, is small (k_H/k_D = 1.120). The secondary isotope effect of H_b, the bystander proton (deuteron), almost in the nodal plane of the carbocation (H_b−C1−C2−C4 = 5.2°), is close to unity (k_H/k_D = 0.996), which suggests that the change in hybridization at C1 between **15** and **16** is small.

The high symmetry (excluding the methyl orientations) of intermediate **18** determines that migration of H_a and H_b is equally favored. The primary and secondary isotope effects for hydride migration were determined for **18** → **19** by replacing H_a and H_b respectively, with deuterium. The calculated primary isotope effect for hydride/deuteride migration is k_H/k_D = 2.401 and is nearer the higher end of the primary kinetic isotope values (1.2−3.0) observed experimentally for 1,2-hydride shifts.[21] A large inverse secondary isotope effect was calculated, k_H/k_D = 0.859, for the hydride/deuteride shift between **18** and **19**. The hybridization in **18** is sp^3 but modified by H_a and H_b hyperconjugation with the C2 cation. For transition structure **19**, the migrating proton is positioned close to midway between C1 and C2 and hybridization at carbon between sp and sp^2 character. Isotopically sensitive vibrational modes that increase in frequency in proceeding from reactant to transition structure are responsible for inverse secondary isotope effects.[25]

The vibrational frequencies responsible for the secondary isotope effects between the nondeuterated and deuterated transition structure **19** and intermediate **18** are presented in Table 4.

The C−H stretching modes for transition structure **19** and intermediate **18** show the greatest variation upon isotopic substitution and in each case reduce in frequency on isotopic substitution. These frequencies are character-

(21) Experimentally determined deuterium isotope effects for 1,2-hydride shifts, where bending vibrations are important, lie in the range of 1.2−3.0. Myhre, P. C.; Brown, K. S. *J. Am. Chem. Soc.* **1969**, *91*, 56391. Myhre, P. C.; Evans, E. *J. Am. Chem. Soc.* **1969**, *91*, 5641. Karabatsos, G. J.; Hsi, N.; Meyerson, S. *J. Am. Chem. Soc.* **1970**, *92*, 621. Karabatsos, G. J.; Mount, R. A.; Rickter, D. O.; Meyerson, S. *J. Am. Chem. Soc.* **1970**, *92*, 1248.

(22) Truhlar, D. G. Isaacson, A. D.; Garrett, B. C. In *The Theory of Chemical Reaction Dynamics*; Baer, M., Ed.; CRC Press: Boca Raton, FL, 1985; Chapter 2. Gonzalez-Lafont, A.; Truong, T. N.; Truhlar, D. G. *J. Chem. Phys.* **1991**, *95*, 8875. Truhlar, D. G.; Steckler, R.; Gordan, M. S. *Chem. Rev.* **1987**, *87*, 217. Schatz, G. C.; *Chem. Rev.* **1987**, *87*, 81.

(23) Bell, R. P. *The Tunnel Effect in Chemistry*; Chapman and Hall: New York, 1980; p 61.

(24) Blackett, B. N.; Coxon, J. M.; Hartshorn, M. P.; Jackson, B. L. J.; Muir, C. N. *Tetrahedron* **1969**, *25*, 1479.

(25) Inverse α-deuterium secondary isotope effects are not uncommon for $sp^3 \rightarrow sp^2$ processes and bimolecular S_N2 reactions at methyl have been reported to be as low as 0.87. Llewellyn, J. A.; Robertson, R. E.; Scott, J. W. M. *Can. J. Chem.* **1960**, *38*, 222.

Table 2. Energies of stationary points (ZPC scaled by 0.961 (B3LYP) and 0.893 (HF))

		energy (au)	ZPC (au)	energy + scaled ZPC (au)	imaginary frequencies. (i cm^{-1})	energy relative to minima **21**
			Transition Structure			
BF_3						
22	optimized					
	HF/6-31G*	−554.12414	0.13573	−554.00294	188.2	23.2
	B3LYP/6-31G*	−556.96517	0.12692	−556.84320	231.0	22.4
		−556.97626[a]				20.8
24	optimized					
	HF/6-31G*	−554.11428	0.13471	−553.99398	115.1	28.8
	B3LYP/6-31G*	−556.95532	0.12521	−556.83499	139.7	27.6
		−554.97200[a]				23.5
25	optimized					
	HF/6-31G*	−554.11408	0.13454	−553.99394	129.7	28.9
	B3LYP/6-31G*	−556.95462	0.12526	−556.83425	128.5	28.0
		−556.96928[a]				25.2
27	optimized					
	HF/6-31G*	−554.11823	0.13282	−553.99962	635.8	25.3
	B3LYP/6-31G*	−556.96058	0.12372	−556.84169	333.3	23.4
		−556.97709[a]				20.3
28	optimized					
	HF/6-31G*	−554.11914	0.13284	−554.00051	763.6	24.7
	B3LYP/6-31G*	−556.95969	0.12365	−556.84086	615.5	23.9
		−556.97528[a]				21.5
30	optimized					
	HF/6-31G*	−554.11632	0.13300	−553.99755	30.9	26.6
	B3LYP/6-31G*	−556.95742	0.12352	−556.83872	55.8	25.2
		−556.97909[a]				19.1
			Minima			
BF_3						
21	optimized					
	HF/6-31G*	−554.16294	0.13776	−554.03992		0.0
	B3LYP/6-31G*	−557.00282	0.12890	−556.87895		0.0
		−557.00948[a]				0.0
26	optimized					
	B3LYP/6-31G*	−556.96335	0.12439	−556.84382		22.0
		−556.97772[a]				19.9
29	optimized					
	HF/6-31G*	−554.19794	0.13697	−554.07563		−22.4
	B3LYP/6-31G*	−557.03104	0.12827	−556.90777		−18.1
		−557.03710[a]				−17.3
23	optimized					
	HF/6-31G*	−554.18654	0.13953	−554.06194		−13.8
	B3LYP/6-31G*	−557.02071	0.13055	−556.89526		−10.2

[a] B3LYP/6-31G* (SCI-PCM) single point calculations. A dielectric constant of 2.23 (CCl_4) was used at 298.15 K.

Table 3. Primary and Secondary Isotope Effects for Hydride Migration

		geometric parameters		isotope effects (k_H/k_D)	
process	ΔE (TS − Min) (kcal/mol)[a,b]	H_{mig}−C1 bond length[a] (Å)	H_{mig}-C1-C2 bond angle[a] (deg)	PIE[c]	SIE[c]
H^+					
15 → TS **16**	2.7[a]/4.6[b]	1.100	109.6	1.120	0.996
18 → TS **19**	5.1[a]/5.0[b]	1.245	67.7	2.401	0.859
BF_3					
21 → TS **24**	27.6[a]/23.5[b]	1.111	105.4	1.202	1.022
26 → TS **27**	1.4[a]/0.4[b]	1.167	83.7	1.995	0.892
26 → TS **28**	1.9[a]/1.6[b]	1.211	73.7	2.092	0.902
30 → TS **27**	−1.8[a]/1.2[b]	1.167	83.7	1.677	0.811
30 → TS **28**	−1.3[a]/2.4[b]	1.211	73.7	1.898	0.760

[a] B3LYP/6-31G*. [b] B3LYP/6-31G*/(SCI−PCM) calculated at 298.15 K with $\epsilon = 2.23$ (CCl_4). [c] Isotope effects calculated with B3LYP/6-31G* optimized geometries and frequencies.

ized as C1−H_a = 3036 cm^{-1} and C1−D_a = 2329 cm^{-1} in **19** and C1−H_a = 2924 cm^{-1} and C1−D_a = 2146 cm^{-1} in **18**. The frequencies for **19** are 112−185 cm^{-1} greater than in the latter. These larger frequencies in **19** are consistent with the transition structure H−C(sp^2) bonds being stronger than the reactant **18** H−C(sp^3) bonds. The difference between the C−H_a and C−D_a stretching frequencies in **18** is larger (878 cm^{-1}) than for **19** (707 cm^{-1}) and this would give a normal contribution to the overall secondary isotope effect.

The out-of-plane bending frequencies at C1 for **19** and **18** also show a decrease with isotopic substitution but less than for the C1−H(D) stretching modes. The nondeuterated and deuterated out-of-plane bending frequencies at C1−H_a(D_a) are characterized at 1166 and 1070 cm^{-1} for **19** and at 1096 and 1002 cm^{-1} for **18**, respectively (Table 4). These along with the other mid to low range bending frequencies between 1399 and 918 cm^{-1} collectively make a more significant multiplicative contribution to the reduced isotopic partition function of

Table 4. Harmonic Vibrational Frequencies (cm^{-1}) for the SIE between 18 and 19

	transition structure		intermediate	
mode	TS **19** C1−Hα H_a = H	TS **19** C1−Dα H_a = D	Min **18** C1−Hα H_a = H	Min **18** C1−Dα H_a = D
1	3729	3729	3754	3754
2	3186	3186	3195	3195
3	3166	3166	3171	3171
4	3150	3130	3055	3055
5	3130	3122	3023	3023
6	3122	3050	3018	3018
7	3050	3036	2999	2999
8	3036	2329	2930	2925
9	2151	2148	2924	2146
10	1611	1588	1529	1522
11	1525	1522	1513	1511
12	1495	1494	1478	1461
13	1488	1481	1461	1452
14	1467	1467	1429	1428
15	1431	1431	1391	1378
16	1422	1416	1383	1353
17	1399	1338	1353	1334
18	1322	1301	1334	1271
19	1295	1250	1270	1251
20	1262	1201	1240	1199
21	1192	1119	1197	1154
22	1166	1070	1159	1088
23	1079	1014	1096	1002
24	1031	983	1002	959
25	1005	939	950	918
26	902	900	819	819
27	811	792	795	783
28	584	580	711	667
29	509	488	538	535
30	429	425	390	382
31	380	377	383	369
32	299	286	309	308
33	273	270	274	273
34	191	191	200	193
35	127	127	143	141
36	638i	619i	97	94

transition structure **19** [$(S_2/S_1)f_{TS}$] than for the intermediate **18** [$(S_2/S_1)f_{react}$] and are responsible for the inverse secondary isotope effect. This implies that the bending motion of the C1-α-hydrogen/deuterium is more constrained for the sp^2 hybridized transition structure **19** than in the sp^3 hybridized intermediate **18**.

BF_3-Catalyzed Rearrangement of Methylpropene Oxide to Methylpropanal. A study of the potential energy surface of the reaction of methylpropene oxide and BF_3 shows a low-energy pathway from **21** via transition structure **22** to **23** (Figure 4).

The barrier to this rearrangement is considerably higher (22.4 kcal/mol) than that for ring opening of the epoxide with acid (2.7 kcal/mol, Figure 3). Ring opening to transition structure **22** is accompanied by rotation about C1−C2, which positions a fluorine of the BF_3 (C2−F = 2.416 Å) favorably for intramolecular reaction with the C2 cation in a reaction that occurs with retention of configuration. Neither of the C1 hydrogens are positioned to migrate (O−C1−C2−C4 = 69.3°). An IRC calculation on transition structure **22** led to **21** and **23**, the latter involving migration of fluorine from the BF_3 group to C2. Fluorohydrin, which would be the product of work up of such a reaction, is not observed in the experiment.[26] Structure **23** is a weaker Lewis acid

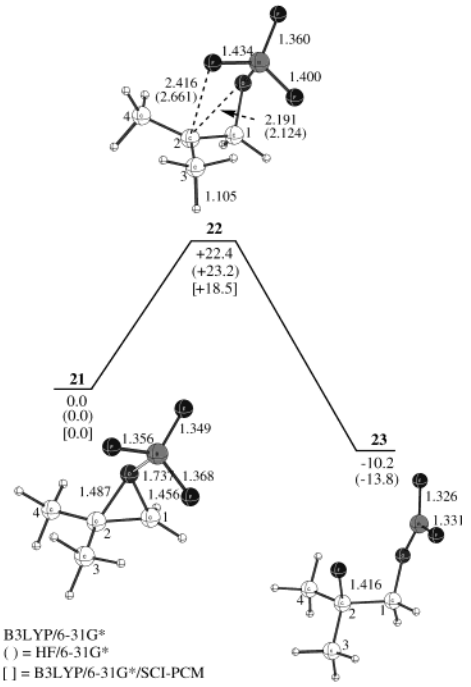

Figure 4. The lowest energy pathway for the rearrangement of epoxide coordinated with BF_3 (**21**) to **23** via transition structure **22**. Bond lengths are in Å with energies relative to **21** in kcal/mol.

than BF_3, and in the absence of more than 1 mol equiv of BF_3, rearrangement to aldehyde would not be expected since **23** is unlikely to act as a Lewis acid catalyst for the removal of the C2−F. The reaction **21** and **23** is exothermic and the activation barrier in the reverse direction is such that the reaction is not expected to be reversible. The fluoro compound **23** therefore does not appear to be on the potential energy surface to aldehyde.

Two further transition structures **24** and **25** on the potential energy surface were established (Figure 5) with activation barriers **21** and **24** (27.6 kcal/mol) and **21** and **25** (28.0 kcal/mol) both higher than that for **21** and **22** (22.4 kcal/mol).

These transition structures are favorable for hydride migration since rotation about C1−C2 positions C1−H_a to overlap with the p-orbital at C2 (**24**, C3−C2−C1−H_a = 74.4°; **25**, C3−C2−C1−H_a = 75.6°). Hyperconjugation is observed in **24** (C2−C1−H_a = 105.4°) but not in **25**. The methyls in the lower energy transition structure **24** have rotated relative to their positions in **21** such that a C4−H exhibits hyperconjugation with the C2 cation and is anti to H_a, which also exhibits hyperconjugation. A C3−H forms an intramolecular H−F bond with the BF_3 group (C3H−F = 1.892 Å, C3H−F = 2.300 Å).

An IRC calculation performed on transition structure **24** led to **21** but failed to converge to a minima in the other direction. The last structure from the IRC calculation (before convergence failure) was optimized by recalculating the force constants. The optimization ran a number of steps with no change in energy and with converged maximum and rms force constants to give structure **26**. A frequency calculation revealed the presence of a very small imaginary frequency (5i cm^{-1}) which can be ignored as an artifact of the calculation. In **26** (Figure 5) a boron−fluorine bond of the BF_3 group is lengthened (1.435 Å) and involved in an intramolecular H−F bond with a C3−H proton (1.918 Å). The C3−H

(26) Fluorohydrins have been reported for reaction of epoxides with BF_3 in ether and are known to rearrange on further reaction with BF_3. Coxon, J. M.; Hartshorn, M. P.; Lewis, A. J.; Richards, K. E.; Swallow, W. H. *Tetrahedron* **1969**, *25*, 4445. Blackett, B. N.; Coxon, J. M.; Hartshorn, M. P.; Richards, K. E. *Tetrahedron* **1969**, *25*, 4999. Coxon, J. M.; Lawrey, M. G. *Chem. Ind.* **1969**, 1558.

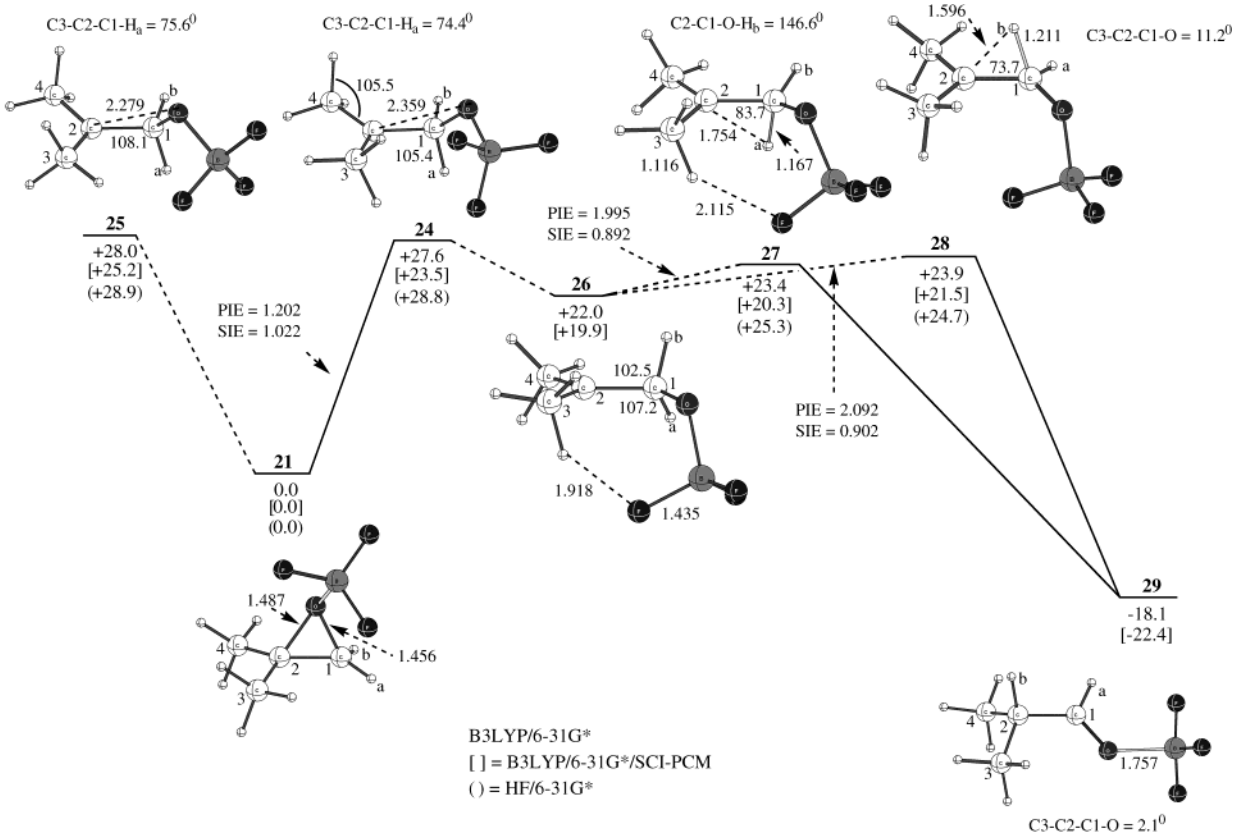

Figure 5. Rearrangement of methylpropene oxide coordinated to BF_3, **21**, to aldehyde. Energies in kcal/mol relative to **21** include a ZPVE correction. All stationary points are optimized at the B3LYP/6-31G* level. Bond lengths are in Å.

proton exhibits hyperconjugation with the C2 cation (H−C3−C2 = 102.6° and C3−H = 1.116 Å). The other methyl has rotated from its conformation in **24** to position a C4−H to hyperconjugate (H−C4−C2 = 107.8°) with the C2 carbocation. The O−C1−C2−C3 torsion in **26** is near planar (3.6°) and H_b is in a more favorable position to hyperconjugate with the cation than H_a (H_b−C1−C2 = 102.5°, C4−C2−C1−H_b = 60.9° and H_a−C1−C2 = 107.2°, C4−C2−C1−H_a = 46.3°).

Two transition structures **27** and **28** for hydride migration (from **26**) were identified (Figure 5). For these structures the OBF_3 has rotated about C1−O (**27**, C2−C1−O−B = 103.2°; **28**, 85.5°) in opposite directions relative to its position in **26** (C2−C1−O−B = 91.0°). While H_b is more favorably positioned to migrate than H_a in **26**, the pathway involving migration of H_a via transition structure **27** is 0.5 kcal/mol lower in energy than the pathway involving H_b via transition structure **28**.[27] For B3LYP/6-31G*-optimized **27**, the H_a−C1−C2 bond angle (83.7°) is reduced and C1−H_a (1.167 Å) lengthened compared with **26** (107.2° and 1.115 Å). Hydride migration is not well-advanced[28] in **27**. Interaction of a C3−H proton with a fluorine is maintained in **27** although weaker with the C3−H−F bond (2.115 Å) longer than in **26** (1.918 Å). Hydride migration in transition structure **28** is more advanced than in **27**, as evidenced by the C2−C1−H_a bond angle (73.7°) and the C1−H_a bond length (1.211 Å). There is less interaction between the BF_3 group and the C3 hydrogen in **28** as a result of rotation of the methyl from its conformation in **26**. Hyperconjugation of the C3−H (H−C3−C2 = 105.0°) and C4−H (H−C4−C2 = 105.9°) with C2 occurs anti to the migrating H_b.

A carbocation structure **30**, akin to the planar protonated carbocation intermediate **18** (Figure 3), was established (Figure 6).

Vibrational frequency analysis confirms **30** as a transition structure due to the presence of a small single imaginary frequency (55i cm^{-1}) and animation of this frequency shows a "wagging" motion of the O−BF_3 group about the O−C1−C2−C3 plane. Structure **30** is planar throughout and is thought to be the transition structure between **26** and its mirror image **26a**. An IRC calculation on **30** did not proceed more than one step along the reaction coordinate in either downhill direction. Although the barrier for interconversion between **26** and **26a** via **30** is small (3.2 kcal/mol, B3LYP/6-31G*), it is higher than the barriers for migration of H_a or H_b from **26** via transition structures **27** and **28** (1.4 and 1.9 kcal/mol), respectively.

Single point SCRF(SCI−PCM) calculations were performed on all the B3LYP/6-31G*-optimized geometries in Figures 5 and 6, and the relative energies are shown in Table 1. A dielectric constant of 2.23 was used for CCl_4 at 298.15 K. The activation barriers leading to the transition structures **24**, **25**, **27**, and **28** are lowered by 2−4 kcal/mol in solvent. While the higher energy gas-phase transition structures **24** and **25** are lowered by the greatest amount in solvent, they still remain the rate-determining steps in the rearrangement of **21**. Of notable interest is the lowering in energy of transition structure

(27) At the HF/6-31G* level, **28** is calculated to be 0.6 kcal/mol higher in energy than **27**, demonstrating the effect of inclusion of electron correlation.

(28) In accord with the Hammond principle, the geometry of **27** is closer to intermediate **26** than to product **29**. Hammond, G. S. *J. Am. Chem. Soc.* **1955**, *77*, 334.

30 (Figure 6) from 25.1 kcal/mol in the gas phase to 19.1 kcal/mol in solvent relative to **21**, which places it slightly lower in energy than the intermediate **26** (19.9 kcal/mol). Although CCl_4 has a low dielectric constant (2.23), the geometry of **30** would favor more charge stabilization at the cationic C2 center by solvent, since there is less steric hindrance from the OBF_3 group than is present in **26**.

Isotope effects were determined for the gas-phase B3LYP/6-31G*-optimized stationary points in Figure 5 by replacing the C1−H_a and C1−H_b protons, respectively, with deuterium. For transition structure **24**, a concerted mechanism for aldehyde formation via a 1,2-hydride shift cannot be excluded since an IRC calculation failed to locate a minima other than **21**. Consequently, a primary and secondary isotope effect was investigated for the rate-determining step from **21** and **24**. The calculated primary isotope effect $k_H/k_D = 1.202$ for H_a is larger than for the rate-determining step **15** and **16** ($k_H/k_D = 1.120$) (Table 3) for protonated methylpropene oxide, consistent with the nearer alignment and hyperconjugation of the H_a proton with the C2 center in **24** ([C3−C2−C1−H_a (74.4°) and C2−C1−H_a (105.4°)] relative to **16** [Figure 3, C3-C2−C1−H_a (59.0°) and C2−C1−H_a (109.6°)]. A small secondary isotope effect was calculated $k_H/k_D = 1.022$ for **21** and **24**, which reflects a modest change in hybridization at C1.

The two competing processes for hydride migration involving the C1−H_a and C1−H_b protons of the nonsymmetrical intermediate **26** were investigated. A primary isotope effect, $k_H/k_D = 1.995$, was calculated for the migration of C1−H_a from intermediate **26** via transition structure **27**. This value is smaller than calculated for the 1,2-hydride shift between protonated **18** and **19** ($k_H/k_D = 2.401$) (Figure 3), showing that hydride migration is less advanced in **27** (H_a−C1−C2 = 83.7° and H_a−C1 = 1.167 Å, Table 3). An inverse secondary isotope effect was calculated ($k_H/k_D = 0.892$) at the C1 center for the process **26** and **27**. The C1−H_b proton exhibits hyperconjugation with the C2 center in **26**, which weakens the bond and results in a distortion from sp^3 hybridization. For **27**, the C1 center exhibits less sp^3 character than in **26** but is not fully sp^2 hybridized, as evidenced by the C2−C1−O−H_b torsional angle of 146.6°. The vibrational frequencies responsible for the secondary isotope effect between the nondeuterated and deuterated transition structure **27** and intermediate **26** are shown in Table 5.

The vibrational modes of particular interest are the C1−H(D) stretching and out-of-plane bending frequencies. For transition structure **27**, isotopic substitution lowers the C1−H_b stretching frequency from 3003 to 2475 cm^{-1} and both of these values are higher than for intermediate **26** (2833 and 2073 cm^{-1}), respectively. However the greater difference between the C1−H_b and C1-D_b frequencies in **26** (760 cm^{-1}) than for **27** (528 cm^{-1}) results in a normal contribution to the overall secondary isotope effect.

A large inverse contribution to the overall secondary isotope effect is provided by a stretching frequency of C1−H_a in **27**, which decreases from 2475 cm^{-1} with H_b adjacent to C1 to 2208 cm^{-1} with D_b adjacent to C1. The nondeuterated and deuterated out-of-plane bending frequencies (H_b) are higher in **27** (1271 and 1158 cm^{-1}) than in **26** (1218 and 1104 cm^{-1}), reflecting tighter bonding at the C1 center in the former. The greater collective multiplicative contribution of the mid to low range bending frequencies for the transition structure **27** than

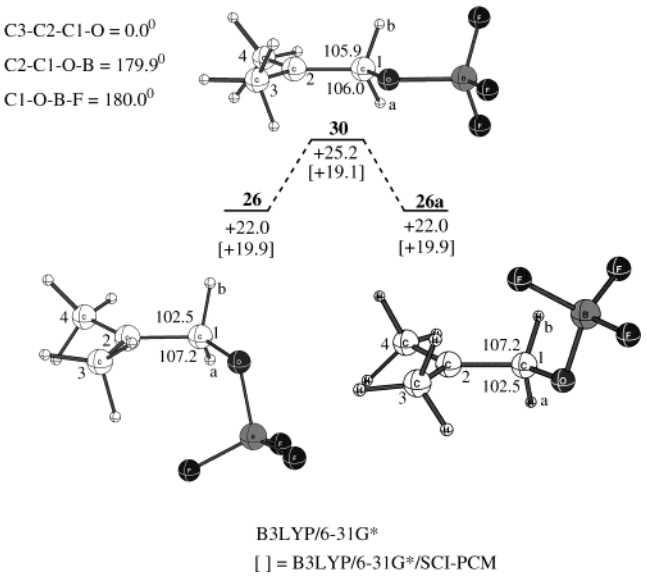

Figure 6. The interconversion of **26** to **26a** via transition structure **30**. Energies (kcal/mol) are relative to BF_3-coordinated epoxide **21**. All stationary points are optimized at the B3LYP/6-31G* level. Bond angles are in degrees.

for the intermediate **26** also provides an inverse contribution to the secondary isotope effect. Tunneling effects do not change the value of the primary and secondary isotope effects for the hydride migration between **26** and **27**, consistent with the very low activation barrier of 1.4 kcal/mol.

The vibrational frequencies for the secondary isotope effect between the nondeuterated and deuterated transition structure **28** and the intermediate **26** are shown in Table 6.

The 1,2-hydride shift between **26** and transition structure **28** involves the C1−H_b, which is more aligned with the C2 p-orbital (H_b−C1−C2−C4 = 60.9°) than the C1−H_a (H_a−C1−C2−C4 = 46.3°) in **26**. The calculated primary isotope effect for C1−H_b migration ($k_H/k_D = 2.092$) was larger than between **26** and **27** ($k_H/k_D = 1.995$), as a consequence of hydride migration being more advanced in the former process. This is illustrated by the smaller C2−C1−H_b bond angle (73.7°) and lengthened C1−H_b bond (1.211 Å) in **28** than in **27** (C2−C1−H_a = 83.7° and C1−H_a =1.167 Å). An inverse secondary isotope effect ($k_H/k_D = 0.902$) was calculated for hydrogen/deuterium placed at the C1−H_a position in **26** and **28**. The C1−H_a stretching frequencies for the nondeuterated (3027 cm^{-1}) and deuterated (2264 cm^{-1}) transition structure **28** (Table 6) are higher than the corresponding modes in intermediate **26** (2833 and 2115 cm^{-1}). The difference between these frequencies is larger for **28** (763 cm^{-1}) than for **26** (718 cm^{-1}) and results in an inverse contribution to the overall secondary isotope effect. The out-of-plane bending mode frequencies for **28** (1287 and 1181 cm^{-1}) are also higher than the corresponding frequencies in **26** (1218 and 1101 cm^{-1}), and the net effect is only a 1% normal contribution to the secondary isotope effect.

B3LYP/6-31G*/SCI−PCM solvent calculations predict transition structure **30** to be lower in energy (19.1 kcal/mol) than intermediate **26** (19.9 kcal/mol) relative to **21**. On the assumption that **30** is a "stable" minimum in solvent, we have investigated isotope effects for hydride

Table 5. Harmonic Vibrational Frequencies (cm^{-1}) for the SIEs between 26 and 27 and 30 and 27

	transition structure		intermediate		intermediate	
mode	TS **27** C1−Hα $H_b = H$	TS **27** C1−Dα $H_b = D$	Min **26** C1−Hα $H_b = H$	Min **26** C1−Dα $H_b = D$	Min **30** C1−Hα $H_b = H$	Min **30** C1−Dα $H_b = D$
1	3175	3175	3184	3184	3178	3178
2	3154	3154	3155	3155	3154	3154
3	3101	3101	3088	3088	3078	3078
4	3059	3059	3059	3059	3038	3038
5	3034	3034	3033	3033	3032	3032
6	3008	3008	2890	2889	3012	3012
7	3003	2475	2866	2866	2809	2795
8	2475	2208	2833	2073	2782	2043
9	1527	1521	1521	1519	1529	1528
10	1516	1513	1512	1511	1507	1506
11	1492	1491	1482	1481	1481	1481
12	1461	1457	1432	1423	1451	1444
13	1455	1437	1421	1409	1444	1444
14	1418	1417	1398	1392	1409	1408
15	1398	1391	1359	1344	1369	1369
16	1364	1322	1347	1328	1330	1318
17	1301	1284	1317	1278	1286	1274
18	1286	1268	1274	1241	1272	1249
19	1271	1158	1246	1227	1248	1199
20	1234	1137	1231	1189	1183	1149
21	1136	1100	1218	1104	1176	1116
22	1119	1069	1103	1084	1123	1074
23	1090	1017	1084	1014	1072	1006
24	1019	1011	1014	982	1006	981
25	1006	952	951	948	976	907
26	890	889	892	871	905	881
27	878	874	809	806	866	866
28	819	795	798	790	827	799
29	736	729	742	721	761	756
30	613	610	677	646	610	609
31	565	561	600	596	607	590
32	503	501	541	534	532	528
33	478	472	505	502	507	506
34	461	460	465	463	437	436
35	386	383	388	387	387	384
36	358	355	368	367	365	362
37	305	304	344	332	301	291
38	286	280	316	312	290	289
39	252	252	302	300	222	218
40	241	236	246	227	219	210
41	195	194	219	215	180	179
42	108	107	171	170	113	106
43	105	105	142	141	107	103
44	26	26	59	58	40	40
45	333i	307i	6i	6i	56i	56i

migration via transition structures **27** and **28** using the frequency data from the gas-phase optimized geometries of **27**, **28**, and **30** (Figure 7).

Although the gas-phase frequency data for **30** show a small imaginary frequency (55i cm^{-1}), it results in no significant contribution to the overall isotope effect and it can essentially be ignored. H_a and H_b in **30** hyperconjugate with the carbocation and are equally positioned to migrate to give aldehyde via a process involving either inversion or retention of configuration. A primary isotope effect for hydride/deuteride placed at the C1−H_a position in **30** and in **27** was calculated to be $k_H/k_D = 1.677$, a result smaller than for **26** and **27** ($k_H/k_D = 1.995$). A large inverse secondary isotope effect was calculated ($k_H/k_D = 0.811$ between **30** and **27** (cf. $k_H/k_D = 0.892$ for **26** and **27**). This result is a consequence of the different vibrational modes associated with **30**, which are displayed in Table 5. The nondeuterated and deuterated C1−H_b and C1−D_b stretching frequencies for **30** (2782 and 2043 cm^{-1}) are lower than the corresponding frequencies in **26** (2833 and 2073 cm^{-1}), respectively. The smaller difference between the C1−H_b and C1−D_b frequencies in **30** (739 cm^{-1}) than in **26** (760 cm^{-1}) reduces the normal contribution to the overall secondary isotope effect from **30** relative to **26**. This is outweighed by the large inverse contribution from the C1−H_a(D_a) stretching frequencies in transition structure **27**.

For the 1,2-hydride shift between **30** and **28**, a primary isotope effect was calculated $k_H/k_D = 1.898$ for migration of H_b, a value smaller than between **26** and **28** ($k_H/k_D = 2.092$). A large inverse secondary isotope effect was calculated ($k_H/k_D = 0.760$) between **30** and **28**, greater than between **26** and **28** ($k_H/k_D = 0.906$). The greater inverse secondary isotope effect is primarily a result of the smaller differences between the nondeuterated and deuterated mid to low range bending frequencies between 1286 and 1006 cm^{-1} in **30** relative to the analogous frequencies in **26** (Table 6). As a result, the contribution to the overall reduced isotopic partition function (S_2/S_1)-f_{react} from these bending frequencies is smaller in **30** than in **26**, therefore resulting in a greater inverse secondary isotope effect for **30** and **28** than for **26** and **28**.

The true k_H/k_D ratio reflecting the 1,2-hydride shift between **2** and **3** and **2** and **4** (Figure 1) requires a correction for the secondary isotope effect introduced by the formation of **4** to be applied to the experimentally

Table 6. Harmonic Vibrational Frequencies (cm^{-1}) for the SIEs between 26 and 28 and 30 and 28

	transition structure		intermediate		intermediate	
mode	TS **28** C1−Hα $H_a = H$	TS **28** C1−Dα $H_a = D$	Min **26** C1−Hα $H_a = H$	Min **26** C1−Dα $H_a = D$	Min **30** C1−Hα $H_a = H$	Min **30** C1−Dα $H_a = D$
1	3173	3173	3184	3184	3178	3178
2	3154	3154	3155	3155	3154	3154
3	3122	3122	3088	3088	3078	3078
4	3111	3111	3059	3059	3038	3038
5	3051	3051	3033	3033	3032	3032
6	3042	3042	2890	2868	3012	3012
7	3027	2264	2866	2832	2809	2793
8	2257	2222	2833	2115	2782	2045
9	1546	1534	1521	1519	1529	1528
10	1520	1517	1512	1510	1507	1506
11	1494	1492	1482	1482	1481	1481
12	1481	1471	1432	1422	1451	1444
13	1464	1460	1421	1410	1444	1444
14	1427	1427	1398	1395	1409	1408
15	1417	1412	1359	1344	1369	1369
16	1378	1344	1347	1321	1330	1317
17	1313	1289	1317	1275	1286	1274
18	1292	1284	1274	1245	1272	1249
19	1287	1181	1246	1231	1248	1199
20	1235	1156	1231	1182	1183	1149
21	1156	1102	1218	1101	1176	1116
22	1149	1092	1103	1076	1123	1073
23	1090	1018	1084	1014	1072	1006
24	1030	1002	1014	969	1006	981
25	1010	954	951	923	976	907
26	892	891	892	890	905	881
27	859	853	809	798	866	866
28	818	795	798	777	827	799
29	700	697	742	740	761	756
30	624	618	677	661	610	609
31	549	540	600	592	607	590
32	498	497	541	535	532	528
33	468	465	505	504	507	506
34	449	434	465	464	437	436
35	391	388	388	386	387	384
36	360	358	368	364	365	362
37	325	315	344	334	301	291
38	288	286	316	314	290	289
39	235	234	302	298	222	218
40	200	200	246	226	219	210
41	182	181	219	218	180	179
42	97	96	171	170	113	106
43	84	83	142	140	107	103
44	30	31	59	58	40	40
45	615i	594i	6i	6i	56i	55i

determined ratio ($M_H/M_D = 1.92$). The correction is presented in the following expressions and it can be shown that the ratio ($M_H/M_D = 1.92$) is required to be multiplied by an appropriate secondary isotope effect.

$$M_H/M_D = \frac{k_{D_{adj}}^{H_{mig}}}{k_{H_{adj}}^{D_{mig}}} \qquad \text{(a)}$$

where the true PIE is

$$\text{PIE} = \frac{k_{H_{adj}}^{H_{mig}}}{k_{H_{adj}}^{D_{mig}}} \qquad \text{(b)}$$

An expression for a SIE is

$$\text{SIE} = \frac{k_{H_{adj}}^{H_{mig}}}{k_{D_{adj}}^{H_{mig}}} \qquad \text{(c)}$$

Substituting eq c into a gives

$$1.92 = \frac{k_{H_{adj}}^{H_{mig}}}{\frac{\text{SIE}}{k_{H_{adj}}^{D_{mig}}}} \quad \text{and} \quad \frac{k_{H_{adj}}^{H_{mig}}}{k_{H_{adj}}^{D_{mig}}} = (1.92)(\text{SIE})$$

The subscripts mig and adj refer to the hydrogen (deuterium) migrating via a 1,2-shift and to the hydrogen (deuterium) adjacent to the reaction center, respectively. From Table 3 and Figure 7, the primary and secondary isotope effects most representative of the true experimental primary isotope effect is that for the process **30** and **27** where a PIE of $k_H/k_D = 1.677$ and a SIE of $k_H/k_D = 0.811$ is calculated. Multiplying the latter with the experimental ratio ($M_H/M_D = 1.92$) gives the corrected experimental primary isotope effect of $k_H/k_D = 1.557$. This value is close to the calculated primary isotope effect $k_H/k_D = 1.677$, and its low magnitude indicates that hydride (deuteride) migration is not fully advanced in the transition structure leading to aldehyde formation.

Conclusion

The present study has established the origins of isotope effects for a 1,2-hydride (deuteride) shift through analysis of the vibrational frequencies of reactant and transition structure. The primary isotope effects largely result from differences between the C1−H(D) stretching frequencies between reactant and transition structure which decrease upon isotopic substitution. Inverse secondary isotope effects were calculated and are attributed to a combination of changes in C1−H(D) stretching and out-of-plane

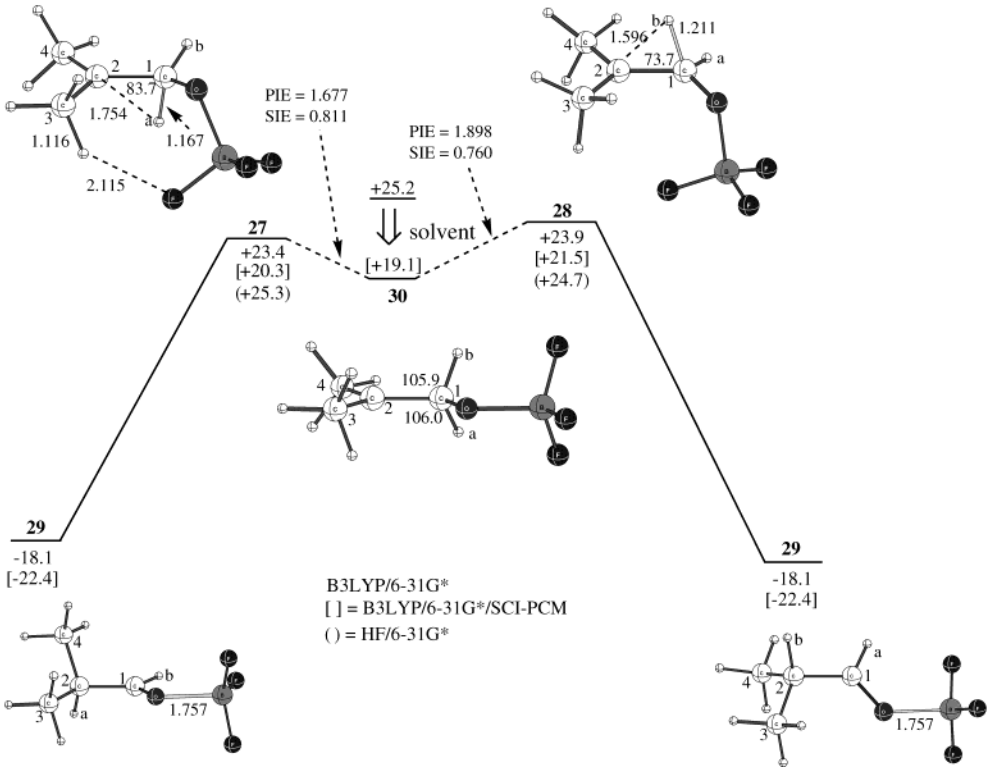

Figure 7.

bending frequencies, and the importance of each varies between the substrates. In all cases these frequencies are lower in the reactant than the transition structure, reflecting tighter force constants and stronger H−C1(sp^2) bonds at the transition structure than the H−C1(sp^3) bonds in the reactant. The calculations support a 1,2-hydride shift from an intermediate **30** (Figure 7), where hydride migration is equally favored to occur with inversion or retention of configuration via an "early" transition structure **27**, where the migrating hydride (deuteride) is not equally positioned between C1 and C2. A calculated correction applied to the experimentally observed result (M_H/M_D = 1.92) results in a primary isotope effect for the reaction (k_H/k_D = 1.557) close to the theoretically calculated value (k_H/k_D = 1.677).

Acknowledgment. We acknowledge grants from the New Zealand Lotteries Board and New Zealand Government Marsden Fund. We also wish to acknowledge helpful discussions on isotope effects with Professor Arvi Rauk, University of Calgary, Calgary, Canada.

Supporting Information Available: Archive material on all stationary points. This material is available free of charge via the Internet at http://pubs.acs.org.

JO9911802